

# To Call or Not to Call: Diagnosing Intrinsic Over-Calling Bias in LLM Agents

Wei Shi<sup>1,2\*</sup>, Ziheng Peng<sup>2,3\*</sup>, Sihang Li<sup>5</sup>, Xiting Wang<sup>3</sup>,  
Xiang Wang<sup>5</sup>, Mengnan Du<sup>4</sup>, Na Zou<sup>2†</sup>

<sup>1</sup>Shanghai Jiao Tong University, <sup>2</sup>Shanghai Artificial Intelligence Laboratory,  
<sup>3</sup>Renmin University of China, <sup>4</sup>The Chinese University of Hong Kong Shenzhen,  
<sup>5</sup>University of Science and Technology of China,  
shiwei1@pjlab.org.cn, mengnandu@cuhk.edu.cn,  
{ziheng.peng, xitingwang}@ruc.edu.cn,  
{sihang0520, xiangwang1223, zouna891252}@gmail.com

## Abstract

LLM agents exhibit a consistent tendency to over-call, invoking tools even in situations where none is needed. On the When2Call benchmark, six models from three families show high call accuracy but much lower no-call accuracy, leaving overall accuracy in the 55%–70% range. We trace this to an Intrinsic Bias Hypothesis (**IBH**): the call/no-call decision mapping carries an activation-independent CALL offset, so the model favors CALL even at activation parity. Using Sparse Autoencoders (SAEs), we recover behavior-aligned feature bases for the CALL/NO\_CALL decision, reduce them to a signed activation margin, and estimate the offset directly. Across all six models, the model is decision-neutral only when NO\_CALL activation outweighs CALL activation, consistent with IBH. We then causally test IBH with Adaptive Margin-Calibrated Steering (**AMCS**), a closed-form counter-bias shift along SAE decoder directions. Cancelling the diagnosed offset mitigates over-calling and improves overall accuracy with a negligible drop in call accuracy. Our work recasts over-calling from an empirical phenomenon into a mechanistic object amenable to causal correction. The code is available at <https://github.com/SKURA502/agent-sae/>.

## 1 Introduction

Large language models (LLMs) have rapidly evolved from text generators into the reasoning backbone of autonomous agents [1–4]. At the core of this transition lies tool use, the ability to interface with external systems such as search engines, code interpreters, APIs, and databases, extending LLMs beyond pure language modeling [5–8].

Beyond executing calls correctly, effective tool use hinges on knowing when to invoke a tool and, crucially, when not to. As shown in Figure 1(a), across six models from three families (Qwen3.5 [4], Gemma-3 [9], Ministral-3 [10]) evaluated on the When2Call benchmark [11], call accuracy remains high, while no-call accuracy is consistently much lower, leaving overall accuracy in the 55%–70% range. Models therefore know how to call tools when calls are required, but often issue calls when none is warranted. Figure 1(a) illustrates this failure mode: given an underspecified Spotify request, the base model invokes the tool instead of asking for the missing song name and device ID. This bias degrades user experience and inflates API costs in deployed systems.

\*Equal Contribution

†Corresponding

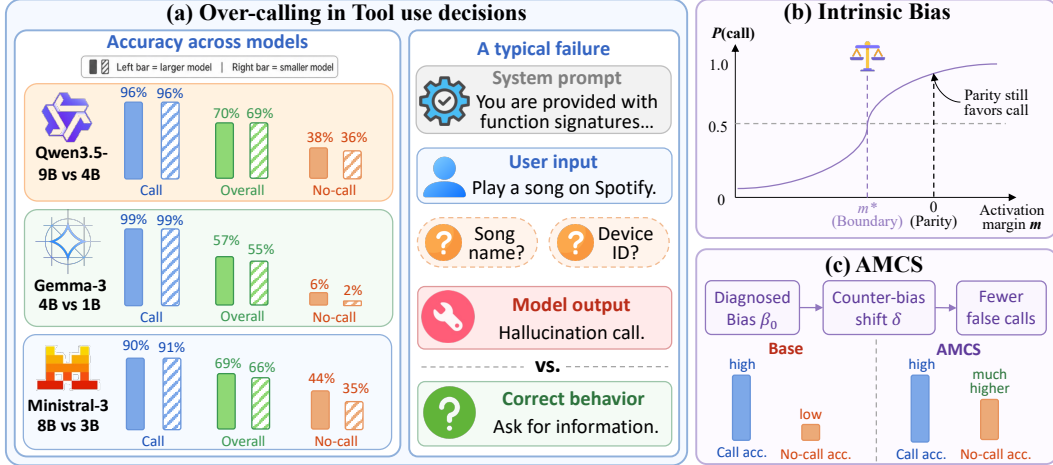


Figure 1: **Overview of over-calling, intrinsic bias, and AMCS.** (a) Across six target models, **call accuracy** is high, but **no-call accuracy** is much lower, reducing **overall accuracy**; a representative case shows the model calling a tool despite missing required information. (b) **Intrinsic Bias Hypothesis**: at activation parity ( $m = 0$ ), the decision still favors CALL; the neutral boundary shifts to  $m^* < 0$ . (c) **AMCS** converts the diagnosed bias  $\beta_0$  into a counter-bias shift  $\delta$ , aiming to reduce false calls while preserving valid calls.

Having documented the bias, we ask what governs the call/no-call decision. An activation-only account offers a natural mechanism: the decision is determined by the relative activation of call- and no-call-related directions, with the stronger side prevailing. This account makes a testable prediction. If the decision depends only on the activation difference, balancing call and no-call activation should leave the model decision-neutral. Our analysis shows the opposite. Even at activation parity, the model remains biased toward CALL; it becomes neutral only when no-call activation is stronger. A residual bias at parity cannot come from activation levels themselves and must instead enter the decision through a separate, additive term. We formalize this as the **Intrinsic Bias Hypothesis (IBH)**: over-calling reflects an activation-independent call offset in the decision mapping.

We test IBH through a pipeline built on Sparse Autoencoders (SAEs) [12, 13], which decompose residual-stream activations into sparse and interpretable features [12, 14] and let us isolate the components driving the CALL/NO\_CALL decision. We first recover behavior-aligned CALL and NO\_CALL feature bases and verify that a handful of them predict the decision near the residual-stream upper bound (§3). We then reduce these bases to a signed activation margin and test whether activation parity removes the decision asymmetry (§4). It does not: activation geometry and logistic estimates of the offset both show a shifted neutral boundary (Figure 1(b)), and the same SAE directions also separate true from false calls, exposing a lever for intervention. Finally, we causally test IBH with Adaptive Margin-Calibrated Steering (**AMCS**), a closed-form counter-bias shift along SAE decoder directions (§5; Figure 1(c)). Cancelling the diagnosed offset raises no-call accuracy by 4–17 points on five of six models and overall accuracy by up to 5 points, with minimal impact on call accuracy across the same models.

Our main contributions are:

- We open a mechanistic view of tool-use gating by recovering behavior-aligned SAE feature bases that predict the CALL/NO\_CALL decision near the residual-stream upper bound (§3).
- We formulate and validate **IBH**, showing that over-calling reflects an activation-independent call offset rather than activation levels alone, and that the same SAE directions further separate true from false calls (§4).
- We introduce **AMCS**, a closed-form steering method derived from the diagnosed offset, and use it as a causal validation of **IBH** that mitigates over-calling across six models from three families with minimal impact on valid tool calls (§5).

## 2 Related Work

### 2.1 Tool-Use Evaluation and the Over-Calling Phenomenon

LLM agents have evolved from early API and calculator integrations [5, 15, 16] to systems spanning large collections of real-world tools [6]. A corresponding evaluation ecosystem studies whether models can invoke tools correctly: selecting the right function, producing valid arguments, and completing tool-mediated tasks [7, 17, 18]. These benchmarks measure how well models call tools, but the gating question of when not to call is less central. When2Call [11] targets this decision directly and reveals a consistent asymmetry: models perform much better on call-required queries than on queries where not calling a tool is correct. Rather than another benchmark or data-side remedy, we ask what internal mechanism produces this asymmetry and diagnose over-calling as a measurable bias in the model’s decision mapping.

### 2.2 Mechanistic Interpretability and Sparse Autoencoders

Understanding why over-calling arises requires tools that can dissect a model’s internal computations. Mechanistic interpretability [19] provides this foundation, aiming to decompose model behavior into interpretable internal components and identify the structures responsible for specific outputs. Within this framework, Sparse Autoencoders (SAEs) have become a widely adopted method for recovering sparse, interpretable units from residual streams [12, 20, 14], with variants such as TopK [13] and JumpReLU [21] improving reconstruction fidelity and feature quality.

We use SAEs to extract a structured feature basis for testing a mechanistic hypothesis. The same basis supports both estimating an activation-independent call offset and applying a counter-bias intervention along these directions as a causal test of the diagnosed offset.

## 3 Discovering Gating Feature Bases

Testing IBH requires a feature basis that reliably indexes the model’s call/no-call decision. We construct two such bases,  $\mathcal{C}$  and  $\mathcal{N}$ , by training SAEs on residual streams (§3.1), ranking features by the model’s observed call/no-call behavior (§3.2), and validating them with linear probes (§3.3).

### 3.1 SAE Training

We train a separate TopK SAE [13] for each of six target models from three families at two scales: Qwen3.5-(4B, 9B), Gemma-3-it-(1B, 4B), and Ministral-3-Instruct-(3B, 8B). Given a residual-stream activation  $\mathbf{h} \in \mathbb{R}^d$ , the encoder and decoder compute:

$$\mathbf{z} = \text{TopK}(\mathbf{W}_{\text{enc}}(\mathbf{h} - \mathbf{b}_{\text{pre}})) \in \mathbb{R}^M, \tag{1}$$

$$\hat{\mathbf{h}} = \mathbf{W}_{\text{dec}} \mathbf{z} + \mathbf{b}_{\text{pre}}, \tag{2}$$

where  $M = 8d$ ,  $K = \lfloor d/32 \rfloor$ , and the columns of  $\mathbf{W}_{\text{dec}} \in \mathbb{R}^{d \times M}$  are constrained to unit norm. Training minimizes the reconstruction loss  $\mathcal{L} = \|\mathbf{h} - \hat{\mathbf{h}}\|_2^2$ . Each SAE is hooked at the output residual stream of a middle-to-late transformer block of its target model, where representations are sufficiently abstract for high-level decision features to emerge. Training follows a two-stage curriculum. Stage 1 trains on OpenWebText2 [22] ( $\approx 50\text{M}$  tokens) to learn a broad sparse feature basis grounded in general residual-stream geometry. We use this broad-corpus stage to reduce the risk that a narrow, domain-specific initialization leaves gaps in residual-stream coverage. Stage 2 continues on the When2Call training split ( $\approx 10\text{M}$  tokens) to adapt the dictionary to tool-use contexts while retaining the broad coverage from Stage 1. Training details, model-specific hook locations, and diagnostics are reported in Appendix A.

### 3.2 Behavior-Labeled Feature Ranking

**Dataset and behavioral labeling.** We build the discovery set from the When2Call evaluation split [11], using all contexts regardless of the original category. For each context  $x_i$ , we run the target LLM  $f_\theta$  to obtain a response  $y_i$  and use an independent LLM judge to classify  $y_i$  into one of the four When2Call response types (judge prompt in Appendix B). Responses judged as `tool_call` form

$\mathcal{D}^+$  (CALL) and responses judged as `request_for_info` from  $\mathcal{D}^-$  (NO\_CALL). Responses in the other two categories are excluded. Each  $(x_i, d_i)$  records the model’s observed gating decision rather than an external correctness label. Per-model response-label counts are reported in Appendix C.

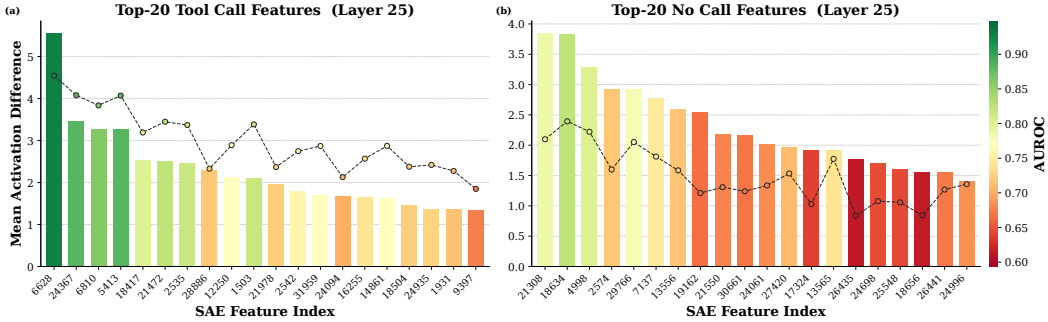


Figure 2: Top-ranked gating features discovered for Qwen3.5-9B. Bars show the mean activation difference between the target and contrast behavior-labeled sets, and the dashed line shows directional AUROC. Left: features associated with observed CALL decisions. Right: features associated with observed NO\_CALL decisions.

**Feature extraction and ranking.** For each  $x_i \in \mathcal{D}$ , we extract the residual-stream activation  $\mathbf{h}_i$  at the action-boundary position, *i.e.*, the position of the final prompt token before the first generated response token. We encode  $\mathbf{h}_i$  with Eq. (1) to obtain SAE activation  $\mathbf{z}_i \in \mathbb{R}^M$ . We first identify CALL features by treating  $\mathcal{D}^+$  as the target set and  $\mathcal{D}^-$  as the reference set. For each SAE feature  $j$ , we compute the mean activation gap and the directional AUROC:

$$\Delta\text{CE}_{\mathcal{C}}(j) = \mathbb{E}_{\mathcal{D}^+}[z_j] - \mathbb{E}_{\mathcal{D}^-}[z_j], \quad (3)$$

$$\text{AUROC}_{\mathcal{C}}(j) = P(z_j(x^+) > z_j(x^-)), \quad x^+ \sim \mathcal{D}^+, x^- \sim \mathcal{D}^-. \quad (4)$$

For a ranking cutoff  $R$ , we keep the intersection of the top- $R$  features under the two scores. The intersection favors features that are both strongly separated in mean activation and consistently discriminative across examples. The CALL pass yields  $\mathcal{C}$ . We obtain the NO\_CALL feature set  $\mathcal{N}$  by the same procedure after swapping the target and reference sets, using  $\mathcal{D}^-$  against  $\mathcal{D}^+$ . Sweeping  $R$  gives the accuracy-sparsity trade-off used in validation.

Figure 2 shows the resulting top-ranked features for Qwen3.5-9B. Both panels exhibit features with large activation gaps and high directional AUROC, indicating that the discovered features are not artifacts of a small number of extreme activations. Analogous results for the remaining target models are reported in Appendix D.

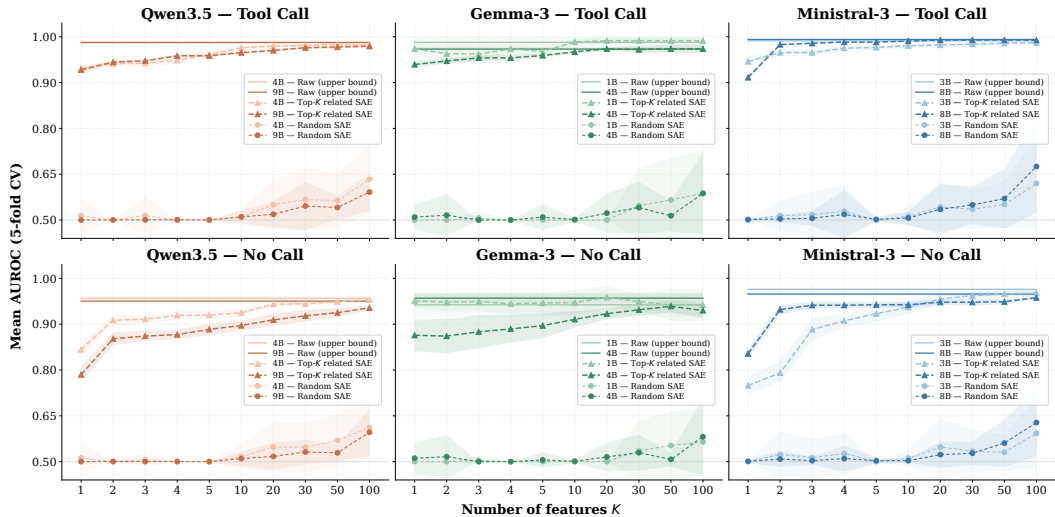


Figure 3: Discriminative validation across six target models. We train 5-fold cross-validated logistic probes with increasing numbers of selected SAE features and report mean AUROC.

### 3.3 Discriminative Validation

**Probe setup.** We validate the discovered features by testing whether a small linear probe trained on them predicts the model’s behavior-labeled gating decision. For a selected feature set  $\mathcal{S}$ , we train a logistic regression on the sparse activations  $\mathbf{z}_{\mathcal{S},i} = (z_j)_{j \in \mathcal{S}}$  at the action-boundary position:

$$\hat{d}_i = \sigma(\mathbf{w}^\top \mathbf{z}_{\mathcal{S},i} + b), \quad (5)$$

where  $\sigma$  is the sigmoid function. Under 5-fold cross-validation, we compare three feature inputs: the top-ranked discovered SAE features, count-matched random SAE features, and the raw residual stream  $\mathbf{h}_i$ , where the last serves as an upper bound. We sweep the number of selected features  $|\mathcal{S}|$  and report mean AUROC across folds.

**Observation 1: A handful of discovered features predict the gating decision near the residual-stream upper bound.** Figure 3 plots mean AUROC as  $|\mathcal{S}|$  grows. Across all three model families and both call and no-call directions, the discovered features reach the raw-residual upper bound with only a handful of SAE dimensions (typically  $K \leq 5$ ), while count-matched random features stay near chance. This proximity to the upper bound indicates that  $\mathcal{C}$  and  $\mathcal{N}$  capture nearly all of the linearly recoverable gating signal in the residual stream, establishing them as a reliable feature basis. Section 4 uses them to test whether the over-calling bias reduces to activation levels alone.

## 4 Diagnosing Intrinsic Decision Bias

This section diagnoses the mechanism of over-calling by asking whether the model’s CALL preference is fully accounted for by CALL- and NO\_CALL-feature activation levels, and by quantifying any activation-independent component of the decision mapping.

### 4.1 Formalizing the Hypothesis

Section 3 identifies two SAE feature sets,  $\mathcal{C}$  and  $\mathcal{N}$ , that track the model’s CALL and NO\_CALL decisions. Using these features, we ask whether over-calling is fully explained by activation levels, or whether the decision mapping itself carries an activation-independent CALL bias. To make this question testable, we summarize the two feature groups by a signed activation margin and examine the model’s decision as a function of that margin.

For each example  $i$ , let  $z_{j,i}$  denote the activation of SAE feature  $j$  at the action-boundary position. Because SAE decoder columns are unit-norm by construction, feature mean activation can be compared directly in the SAE coordinate space. We define the signed activation margin as the difference between CALL- and NO\_CALL-feature mean activation:

$$m_i = a_{\mathcal{C},i} - a_{\mathcal{N},i} = \frac{1}{|\mathcal{C}|} \sum_{j \in \mathcal{C}} z_{j,i} - \frac{1}{|\mathcal{N}|} \sum_{j \in \mathcal{N}} z_{j,i}. \quad (6)$$

where positive  $m_i$  indicates stronger CALL-feature mean activation and negative  $m_i$  the reverse. Let  $\hat{d}_i = 1$  denote that the model’s response is judged as CALL, and  $\hat{d}_i = 0$  otherwise. The margin gives a direct diagnostic axis on which the two accounts make opposite predictions, formalized below.

**Activation-only account ( $H_{\text{act}}$ ).** The gating decision depends on the activation margin alone:

$$\Pr(\hat{d}_i = 1 \mid m_i) = \sigma(\beta m_i), \quad \beta > 0. \quad (7)$$

**Prediction.** At activation parity,  $\Pr(\hat{d}_i = 1 \mid m_i = 0) = 1/2$ . The neutral decision boundary lies at  $m_i = 0$ .

**Intrinsic Bias Hypothesis ( $H_{\text{IBH}}$ ).** The decision mapping contains an activation-independent CALL offset:

$$\Pr(\hat{d}_i = 1 \mid m_i) = \sigma(\beta m_i + \beta_0), \quad \beta > 0, \quad \beta_0 > 0. \quad (8)$$

**Prediction.** At activation parity,  $\Pr(\hat{d}_i = 1 \mid m_i = 0) = \sigma(\beta_0) > 1/2$ . The neutral boundary shifts to  $m^* = -\beta_0/\beta < 0$ .

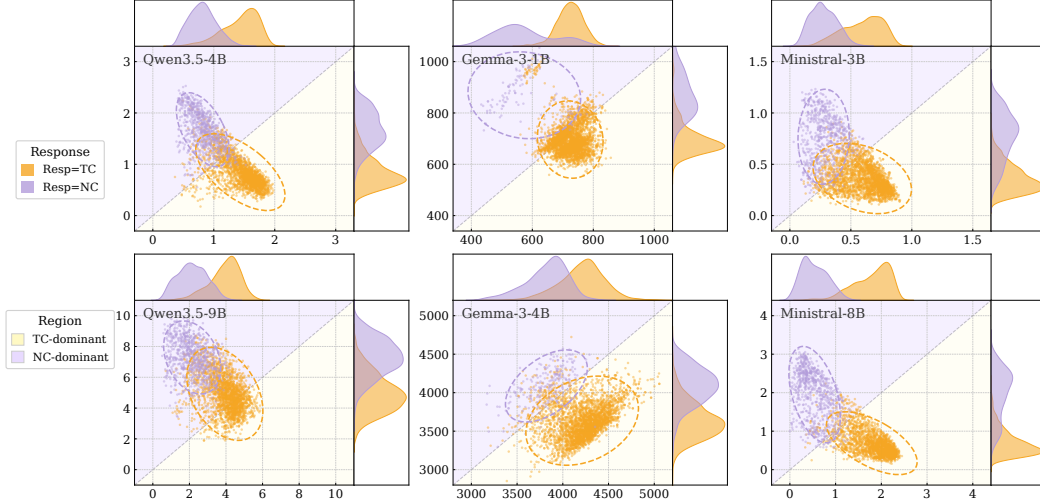


Figure 4: Response-conditioned activation geometry. Examples are grouped by the model’s emitted decision: NO\_CALL responses (purple) stay in the NO\_CALL-dominant half-plane, while CALL responses (orange) extend across the parity diagonal into the same region. The response boundary therefore sits on the NO\_CALL side of the diagonal rather than at activation parity.

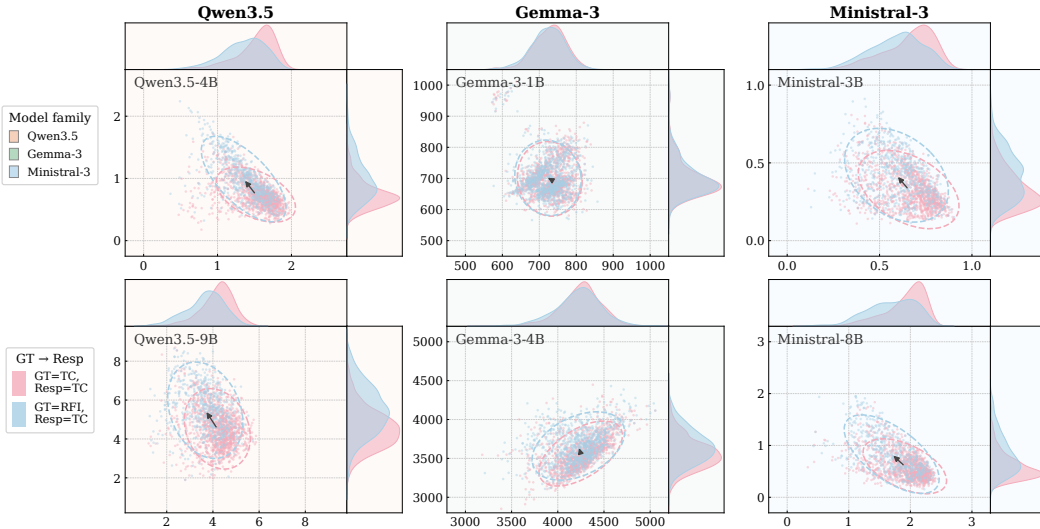


Figure 5: Input-conditioned activation geometry, restricted to examples for which the model emits a CALL. True calls (pink) lie in the CALL-dominant region, while false calls (blue) overlap the same region but sit consistently closer to the parity diagonal. True and false calls therefore remain separable along the  $\mathcal{C}$  and  $\mathcal{N}$  axes within a single emitted decision.

The two accounts therefore disagree on where the model becomes decision-neutral: at activation parity under  $H_{\text{act}}$ , only after NO\_CALL evidence exceeds CALL evidence under  $H_{\text{IBH}}$ . We first examine the activation geometry of CALL- and NO\_CALL-feature evidence from both response- and input-conditioned views, then estimate the offset term  $\beta_0$  directly.

## 4.2 Evidence for Intrinsic Bias

To test these predictions, we examine each example’s feature evidence in the plane  $(a_{\mathcal{C}}, a_{\mathcal{N}})$ , where the diagonal marks  $m = 0$ . We probe this geometry from two complementary views. A response-conditioned view asks whether the parity line separates emitted CALL from NO\_CALL responses. An input-conditioned view then asks whether, among emitted CALL responses, true and false calls share the same feature geometry.

**Observation 2: The response boundary is shifted into the NO\_CALL-dominant half-plane.** Across all six target models (Figure 4), NO\_CALL responses concentrate well inside the NO\_CALL-dominant half-plane, with the model emitting NO\_CALL only when NO\_CALL-feature mean activation clearly exceeds CALL-feature mean activation. CALL responses, by contrast, extend across the parity line into regions where NO\_CALL features are comparable to or stronger than CALL features. This shift is systematic: the model carries a CALL preference that persists even when feature evidence already favors NO\_CALL. This is the directional signature of  $H_{IBH}$ .

**Observation 3: Among emitted calls, false calls lie closer to the NO\_CALL side than true calls.** Conditioning on emitted CALL responses (Figure 5), true and false calls occupy distinct activation distributions: across all six models, the false-call mass sits consistently closer to the parity diagonal than the true-call mass. The same intrinsic CALL preference is therefore still acting inside the CALL subset, pushing examples with weaker CALL evidence over the response boundary. Crucially, true and false calls remain separable along the  $\mathcal{C}$  and  $\mathcal{N}$  axes, giving Section 5 a directional lever: a counter-bias along the SAE decoder directions of  $\mathcal{C}$  and  $\mathcal{N}$  can push the shifted false-call mass back across the boundary while leaving the more deeply  $\mathcal{C}$ -dominant true calls in place.

Together, Observations 2 and 3 establish the qualitative shape of  $H_{IBH}$ : the bias surfaces both in where the response boundary sits and in which emitted calls turn out wrong. We now estimate  $\beta_0$  to make this offset quantitative.

### 4.3 Quantifying the Bias Offset

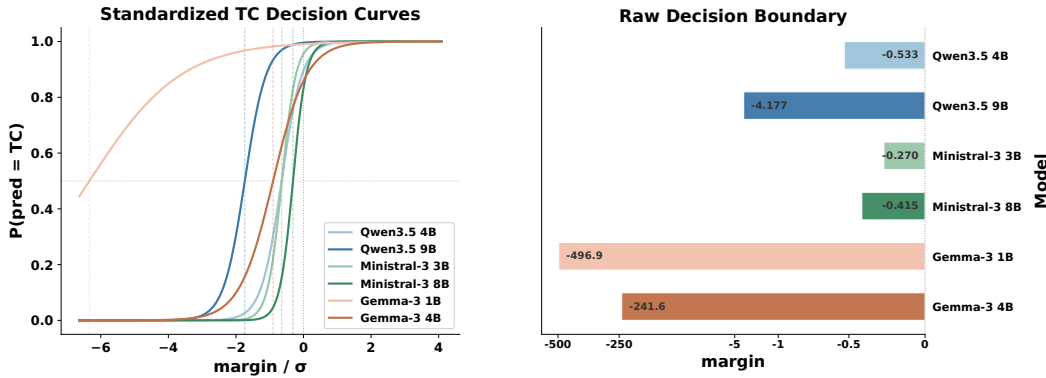


Figure 6: Logistic estimates of intrinsic CALL bias. **Left:** fitted decision curves with margin standardized within model, so the six curves can be visually compared. **Right:** raw neutral boundaries  $\hat{m}^*$ . All boundaries are negative, meaning the model becomes decision-neutral only when NO\_CALL-feature mean activation exceeds CALL-feature mean activation.

For each model, we fit Eq. 8 on cached SAE activations and observed model decisions, yielding empirical estimates  $(\hat{\beta}, \hat{\beta}_0)$ . The intercept  $\hat{\beta}_0$  sets the CALL probability at activation parity, and the neutral boundary  $\hat{m}^* = -\hat{\beta}_0/\hat{\beta}$  marks the margin at which  $\Pr(\hat{d}_i = 1) = 1/2$ . The left panel of Figure 6 expresses margin in within-model standard-deviation units, aligning the six fitted curves: each crosses 0.5 at a negative margin and sits above 0.5 at activation parity. The right panel reports the raw  $\hat{m}^*$ , which are negative for all six models and span several orders of magnitude across families. Across all six models,  $\hat{m}^* < 0$  supports  $H_{IBH}$ : parity between CALL- and NO\_CALL-feature mean activations does not bring the model to decision-neutrality. The much larger raw magnitudes for Gemma likely reflect the larger numerical scale of its activations, so  $\hat{m}^*$  should be read as a within-model bias measure rather than a cross-model strength.

## 5 Causal Steering Experiments

If the offset  $\beta_0$  in Section 4 is part of the mechanism that produces over-calling, counteracting it along the same SAE feature directions should rebalance CALL and NO\_CALL decisions and improve overall accuracy. We instantiate this causal test with Adaptive Margin-Calibrated Steering (AMCS), a closed-form activation steering method derived from the fitted decision-margin model.

## 5.1 Adaptive Margin-Calibrated Steering

**Closed-form calibration.** AMCS reuses the signed activation margin in Eq. (6). For a steering budget of  $r$  features per side, let  $\mathcal{C}_r \subseteq \mathcal{C}$  and  $\mathcal{N}_r \subseteq \mathcal{N}$  denote the top-ranked CALL and NO\_CALL features from Section 3.2. On cached calibration activations and observed model decisions, we refit the diagnostic margin model on this restricted basis using the same margin definition as Section 4.1:

$$\Pr(\hat{d} = 1 \mid m_r) = \sigma(\beta_r m_r + \beta_{0,r}), \quad (9)$$

where  $\hat{d} = 1$  denotes an observed CALL response,  $m_r$  is the signed margin recomputed on  $\mathcal{C}_r \cup \mathcal{N}_r$ , and  $\beta_r, \beta_{0,r}$  are the fitted slope and CALL offset under budget  $r$ . To remove this offset, AMCS shifts every margin by the same amount  $\delta_r$  so that the calibrated logit matches the unbiased one,  $\beta_r(m + \delta_r) + \beta_{0,r} = \beta_r m$  for all  $m$ . This yields the closed-form:

$$\delta_r = -\frac{\beta_{0,r}}{\beta_r}, \quad (10)$$

so the steering strength is fixed by the diagnosed bias rather than tuned on a validation set.

**Steering vector and intervention.** Let  $\mathbf{d}_j$  be the SAE decoder column for feature  $j$ . To allocate the shift across selected features, we measure each feature’s activation gap between CALL-decision and NO\_CALL-decision responses on the calibration set,  $\Delta_j^{\mathcal{C}}$  for  $j \in \mathcal{C}_r$  and  $\Delta_j^{\mathcal{N}}$  for  $j \in \mathcal{N}_r$ , and normalize absolute gaps within each side:

$$\omega_j^{\mathcal{C}} = \frac{|\Delta_j^{\mathcal{C}}|}{\sum_{k \in \mathcal{C}_r} |\Delta_k^{\mathcal{C}}|}, \quad \omega_j^{\mathcal{N}} = \frac{|\Delta_j^{\mathcal{N}}|}{\sum_{k \in \mathcal{N}_r} |\Delta_k^{\mathcal{N}}|}. \quad (11)$$

These weights only set allocation, with the magnitude fixed by  $\delta_r$ . The steering vector is then:

$$\mathbf{v}_r = \underbrace{\alpha r \delta_r \sum_{j \in \mathcal{C}_r} \omega_j^{\mathcal{C}} \mathbf{d}_j}_{\text{CALL suppression } (\delta_r < 0)} + \underbrace{(1 - \alpha) r (-\delta_r) \sum_{j \in \mathcal{N}_r} \omega_j^{\mathcal{N}} \mathbf{d}_j}_{\text{NO_CALL enhancement } (-\delta_r > 0)}, \quad (12)$$

where  $\alpha \in [0, 1]$  trades off the correction between CALL-side and NO\_CALL-side decoder directions, and the factor  $r$  cancels the per-side averaging in  $m_r$  so that  $\mathbf{v}_r$  targets a total margin shift of  $\delta_r$  under a local linear SAE approximation. At inference, we add  $\mathbf{v}_r$  at the SAE hook layer throughout autoregressive generation,  $\mathbf{H}_\ell \leftarrow \mathbf{H}_\ell + \mathbf{v}_r$ , costing one broadcast addition per token. Implementation details are in Appendix E.

## 5.2 Causal Validation Across Models

**Setup.** We evaluate AMCS on When2Call across six instruction-tuned models from three families: Qwen3.5 (4B, 9B), Gemma3 (1B, 4B), and Ministral3 (3B, 8B), reusing the SAE and diagnosis layer of Section 4. AMCS fits  $\beta_r$  and  $\beta_{0,r}$  on a calibration split and is evaluated on a held-out test split, with the balance set to  $\alpha = 0.8$ . We scan the steering budget  $r \in \{5, 10, 15, 20, 25, 30\}$  and report the mean across  $r$ . We compare against three reference interventions, Prompt, Suppress, and Promote, defined in Table 1. The latter two each cover only one half of the AMCS shift, isolating the effect of the closed-form two-sided calibration.

**Results.** Each of the three reference interventions fails in a characteristic way (Table 1). Prompt acts at the surface and overshoots: on Ministral3-8B it raises no-call accuracy by 45 points but cuts tool-call accuracy by 56 points, dropping Overall below *Init*. Suppress and Promote act in the right space but only on one side of the margin: on Qwen3.5-4B, each moves no-call accuracy by under 10 points and Overall by under 3.2 points. AMCS, by combining both sides with magnitude set by  $\beta_0$ , keeps tool-call accuracy within 5 points of *Init* on five of six models<sup>3</sup> while raising no-call accuracy by 4 to 17 points, giving the best Overall on Qwen3.5-4B, Qwen3.5-9B, and Ministral3-3B, and landing within 0.6 points of the best on Ministral3-8B. Cancelling the diagnosed offset  $\beta_0$  along the same SAE directions recovers most of the no-call accuracy that the unmodified model misses, the causal counterpart of IBH.

<sup>3</sup>On the two Gemma3 models, true and false calls show little separation along the  $\mathcal{C}$  and  $\mathcal{N}$  axes (Figure 5), so the SAE feature basis offers little leverage for any margin-based intervention. We report Gemma3 as reference rather than evidence.

Table 1: Causal validation of AMCS on When2Call (%). TC Acc and NC Acc denote tool-call and no-call accuracy. *Init* is the unmodified model. Prompt appends “When the user’s request lacks necessary details, ask before taking action.” to the user prompt. Suppress scales the top-ranked CALL feature activations by 0.5. Promote scales the top-ranked NO\_CALL feature activations by 1.5. Subscripts give the absolute change versus *Init* in percentage points (positive / negative).

Metric	Method	Qwen3.5-4B	Qwen3.5-9B	Gemma3-1B	Gemma3-4B	Ministral3-3B	Ministral3-8B
TC Acc	<i>Init</i>	95.98	96.45	98.61	99.23	91.66	91.97
	Prompt	68.11 <sub>-27.87</sub>	67.72 <sub>-28.73</sub>	94.67 <sub>-3.94</sub>	58.22 <sub>-41.01</sub>	61.62 <sub>-30.04</sub>	35.91 <sub>-56.06</sub>
	Suppress	93.48 <sub>-2.50</sub>	94.61 <sub>-1.84</sub>	93.84 <sub>-4.77</sub>	94.34 <sub>-4.89</sub>	86.75 <sub>-4.91</sub>	85.34 <sub>-6.63</sub>
	Promote	93.82 <sub>-2.16</sub>	96.88 <sub>+0.43</sub>	98.38 <sub>-0.23</sub>	98.53 <sub>-0.70</sub>	90.07 <sub>-1.59</sub>	89.92 <sub>-2.05</sub>
	Ours	91.82 <sub>-4.16</sub>	91.72 <sub>-4.73</sub>	89.77 <sub>-8.84</sub>	99.18 <sub>-0.05</sub>	86.66 <sub>-5.00</sub>	89.90 <sub>-2.07</sub>
NC Acc	<i>Init</i>	37.76	37.57	2.26	5.56	34.65	41.71
	Prompt	77.31 <sub>+39.55</sub>	79.38 <sub>+41.81</sub>	15.91 <sub>+13.65</sub>	59.23 <sub>+53.67</sub>	71.56 <sub>+36.91</sub>	87.10 <sub>+45.39</sub>
	Suppress	44.65 <sub>+6.89</sub>	44.43 <sub>+6.86</sub>	4.35 <sub>+2.09</sub>	7.65 <sub>+2.09</sub>	45.75 <sub>+11.10</sub>	52.75 <sub>+11.04</sub>
	Promote	47.36 <sub>+9.60</sub>	34.27 <sub>-3.30</sub>	2.97 <sub>+0.71</sub>	7.64 <sub>+2.08</sub>	41.26 <sub>+6.61</sub>	46.91 <sub>+5.20</sub>
	Ours	51.07 <sub>+13.31</sub>	54.58 <sub>+17.01</sub>	9.40 <sub>+7.14</sub>	5.55 <sub>-0.01</sub>	45.91 <sub>+11.26</sub>	45.76 <sub>+4.05</sub>
Overall	<i>Init</i>	69.75	69.88	55.20	57.11	65.97	69.33
	Prompt	72.25 <sub>+2.50</sub>	72.97 <sub>+3.09</sub>	59.19 <sub>+3.99</sub>	58.68 <sub>+1.57</sub>	66.10 <sub>+0.13</sub>	58.97 <sub>-10.36</sub>
	Suppress	71.48 <sub>+1.73</sub>	72.00 <sub>+2.12</sub>	53.52 <sub>-1.68</sub>	55.28 <sub>-1.83</sub>	68.27 <sub>+2.30</sub>	70.66 <sub>+1.33</sub>
	Promote	72.89 <sub>+3.14</sub>	68.67 <sub>-1.21</sub>	55.39 <sub>+0.19</sub>	57.58 <sub>+0.47</sub>	68.08 <sub>+2.11</sub>	70.54 <sub>+1.21</sub>
	Ours	73.47 <sub>+3.72</sub>	74.98 <sub>+5.10</sub>	53.56 <sub>-1.64</sub>	57.00 <sub>-0.11</sub>	68.30 <sub>+2.33</sub>	70.10 <sub>+0.77</sub>

## 6 Discussion and Limitations

**Toward controllable calling effort.** Modern LLM interfaces expose knobs for reasoning effort or compute budget, but tool use lacks a comparable control over how readily a model invokes external actions rather than verifying intent with the user. The diagnosed call offset behaves like such a knob: shifting it tunes the balance between eager calling and seeking user verification, without altering the underlying tool-use capability. AMCS is therefore not only a correction for over-calling, but a first step toward a “calling effort” interface where users or systems can set a task-specific point on this call-versus-verify axis.

**Toward agent interpretability.** Interpreting agents requires more than explaining isolated outputs, since real agents act over multiple turns, condition on tool feedback, and update plans dynamically. This paper isolates one consequential unit of that broader problem: the call-versus-verify decision. We connect it to feature-level geometry and a causal intervention, so the mechanism can be measured and adjusted. Extending this analysis to long-horizon agents will require tracking such mechanisms across time, memory, and tool outputs.

**Limitations.** This paper diagnoses and mitigates over-calling in deployed models but does not trace the training-time origin of the bias. AMCS is therefore an inference-time correction, not a training-side fix. Our analysis is further limited by the choice of SAE feature basis and by the local linear approximation that translates decoder-direction interventions into margin shifts. Our empirical study centers on When2Call, leaving downstream agent benchmarks to future work.

## 7 Conclusion

Tool-using LLM agents must decide not only how to call tools, but also when not to call. This paper studied a systematic failure in that decision: models achieve high call accuracy while remaining much less reliable on no-call cases, producing over-calling. Using SAE feature bases for the CALL/NO\_CALL gating decision, we showed that this asymmetry is not fully explained by feature activation levels. We formalized this as IBH: an activation-independent call offset that shifts the neutral boundary toward CALL, so even at activation parity the decision remains biased toward calling.

We then turned this diagnosis into AMCS, a closed-form steering method that counteracts the fitted offset along SAE decoder directions. This unifies behavioral miscalibration, feature-level mechanism, and causal intervention. Over-calling is therefore not only an empirical artifact of tool-use benchmarks. It is a mechanistic object that can be measured, modeled, and causally adjusted.

## References

- [1] OpenAI. Openai GPT-5 system card. *CoRR*, abs/2601.03267, 2026.
- [2] Anthropic. Claude opus 4.6 system card. Technical report, Anthropic, February 2026.
- [3] Google DeepMind. Gemma 4 model card. [https://ai.google.dev/gemma/docs/core/model\\_card\\_4](https://ai.google.dev/gemma/docs/core/model_card_4), April 2026. Accessed: 2026-04-08.
- [4] Qwen Team. Qwen3.5: Accelerating productivity with native multimodal agents, February 2026.
- [5] Timo Schick, Jane Dwivedi-Yu, Roberto Dessi, Roberta Raileanu, Maria Lomeli, Eric Hambro, Luke Zettlemoyer, Nicola Cancedda, and Thomas Scialom. Toolformer: Language models can teach themselves to use tools. In *NeurIPS*, 2023.
- [6] Yujia Qin, Shihao Liang, Yining Ye, Kunlun Zhu, Lan Yan, Yaxi Lu, Yankai Lin, Xin Cong, Xiangru Tang, Bill Qian, Sihan Zhao, Lauren Hong, Runchu Tian, Ruobing Xie, Jie Zhou, Mark Gerstein, Dahai Li, Zhiyuan Liu, and Maosong Sun. Toollm: Facilitating large language models to master 16000+ real-world APIs. In *ICLR*. OpenReview.net, 2024.
- [7] Shishir G. Patil, Tianjun Zhang, Xin Wang, and Joseph E. Gonzalez. Gorilla: Large language model connected with massive APIs. *CoRR*, abs/2305.15334, 2023.
- [8] Jiayi Zhang, Jinyu Xiang, Zhaoyang Yu, Fengwei Teng, Xionghui Chen, Jiaqi Chen, Mingchen Zhuge, Xin Cheng, Sirui Hong, Jinlin Wang, Bingnan Zheng, Bang Liu, Yuyu Luo, and Chenglin Wu. AFlow: Automating agentic workflow generation. In *ICLR*. OpenReview.net, 2025.
- [9] Gemma Team. Gemma 3 technical report. *CoRR*, abs/2503.19786, 2025.
- [10] Mistral AI. Ministral 3. *CoRR*, abs/2601.08584, 2026.
- [11] Hayley Ross, Ameya Sunil Mahabaleshwarkar, and Yoshi Suhara. When2call: When (not) to call tools. In *NAACL (Long Papers)*, pages 3391–3409. Association for Computational Linguistics, 2025.
- [12] Robert Huben, Hoagy Cunningham, Logan Riggs, Aidan Ewart, and Lee Sharkey. Sparse autoencoders find highly interpretable features in language models. In *ICLR*. OpenReview.net, 2024.
- [13] Leo Gao, Tom Dupré la Tour, Henk Tillman, Gabriel Goh, Rajan Troll, Alec Radford, Ilya Sutskever, Jan Leike, and Jeffrey Wu. Scaling and evaluating sparse autoencoders. 2025.
- [14] Adly Templeton, Tom Conerly, Jonathan Marcus, Jack Lindsey, Trenton Bricken, Brian Chen, Adam Pearce, Craig Citro, Emmanuel Ameisen, Andy Jones, Hoagy Cunningham, Nicholas L Turner, Callum McDougall, Monte MacDiarmid, C. Daniel Freeman, Theodore R. Sumers, Edward Rees, Joshua Batson, Adam Jermyn, Shan Carter, Chris Olah, and Tom Henighan. Scaling monosemanticity: Extracting interpretable features from claude 3 sonnet. *Transformer Circuits Thread*, 2024.
- [15] Ehud Karpas, Omri Abend, Yonatan Berant, Barak Lenz, Opher Lieber, Nir Ratner, Yoav Shoham, Hofit Bata, Yoav Levine, Kevin Leyton-Brown, Dor Muhlgay, Noam Rozen, Erez Schwartz, Gal Shachaf, Shai Shalev-Shwartz, Amnon Shashua, and Moshe Tennenholtz. MRKL systems: A modular, neuro-symbolic architecture that combines large language models, external knowledge sources and discrete reasoning. *CoRR*, abs/2205.00445, 2022.
- [16] Shunyu Yao, Jeffrey Zhao, Dian Yu, Nan Du, Izhak Shafran, Karthik R. Narasimhan, and Yuan Cao. React: Synergizing reasoning and acting in language models. In *ICLR*. OpenReview.net, 2023.
- [17] Xiao Liu, Hao Yu, Hanchen Zhang, Yifan Xu, Xuanyu Lei, Hanyu Lai, Yu Gu, Hangliang Ding, Kaiwen Men, Kejuan Yang, Shudan Zhang, Xiang Deng, Aohan Zeng, Zhengxiao Du, Chenhui Zhang, Sheng Shen, Tianjun Zhang, Yu Su, Huan Sun, Minlie Huang, Yuxiao Dong, and Jie Tang. Agentbench: Evaluating llms as agents. In *ICLR*. OpenReview.net, 2024.

- [18] Shishir G. Patil, Huanzhi Mao, Fanjia Yan, Charlie Cheng-Jie Ji, Vishnu Suresh, Ion Stoica, and Joseph E. Gonzalez. The berkeley function calling leaderboard (BFCL): from tool use to agentic evaluation of large language models. In *ICML, Proceedings of Machine Learning Research*. PMLR / OpenReview.net, 2025.
- [19] Lee Sharkey, Bilal Chughtai, Joshua Batson, Jack Lindsey, Jeffrey Wu, Lucius Bushnaq, Nicholas Goldowsky-Dill, Stefan Heimersheim, Alejandro Ortega, Joseph Isaac Bloom, Stella Biderman, Adrià Garriga-Alonso, Arthur Conmy, Neel Nanda, Jessica Rumbelow, Martin Wattenberg, Nandi Schoots, Joseph Miller, William Saunders, Eric J. Michaud, Stephen Casper, Max Tegmark, David Bau, Eric Todd, Atticus Geiger, Mor Geva, Jesse Hoogland, Daniel Murfet, and Tom McGrath. Open problems in mechanistic interpretability. *Trans. Mach. Learn. Res.*, 2025, 2025.
- [20] Trenton Bricken, Adly Templeton, Joshua Batson, Brian Chen, Adam Jermy, Tom Conerly, Nick Turner, Cem Anil, Carson Denison, Amanda Askell, Robert Lasenby, Yifan Wu, Shauna Kravec, Nicholas Schiefer, Tim Maxwell, Nicholas Joseph, Zac Hatfield-Dodds, Alex Tamkin, Karina Nguyen, Brayden McLean, Josiah E Burke, Tristan Hume, Shan Carter, Tom Henighan, and Christopher Olah. Towards monosemanticity: Decomposing language models with dictionary learning. *Transformer Circuits Thread*, 2023.
- [21] Senthoran Rajamanoharan, Tom Lieberum, Nicolas Sonnerat, Arthur Conmy, Vikrant Varma, János Kramár, and Neel Nanda. Jumping ahead: Improving reconstruction fidelity with jumprelu sparse autoencoders. *CoRR*, abs/2407.14435, 2024.
- [22] Leo Gao, Stella Biderman, Sid Black, Laurence Golding, Travis Hoppe, Charles Foster, Jason Phang, Horace He, Anish Thite, Noa Nabeshima, Shawn Presser, and Connor Leahy. The pile: An 800gb dataset of diverse text for language modeling. *CoRR*, abs/2101.00027, 2021.
- [23] Ilya Loshchilov and Frank Hutter. Decoupled weight decay regularization. In *ICLR (Poster)*. OpenReview.net, 2019.

## A SAE Training Details

Table 2: SAE training configuration for each target model.  $d$  is the text-backbone residual width,  $L$  is the number of transformer blocks,  $\ell$  is the zero-indexed hook block,  $M = 8d$  is the SAE dictionary size, and  $K = \lfloor d/32 \rfloor$  is the TopK sparsity.

Model	$d$	$L$	$\ell$	$M$	$K$
Qwen3.5-4B	2560	32	25	20480	80
Qwen3.5-9B	4096	32	25	32768	128
Gemma-3-1b-it	1152	26	17	9216	36
Gemma-3-4b-it	2560	34	29	20480	80
Ministral-3-3B-Instruct	3072	26	21	24576	96
Ministral-3-8B-Instruct	4096	34	31	32768	128

We train SAEs on the text-backbone residual stream of each target model. Following the  $M = 8d$  and  $K = \lfloor d/32 \rfloor$  configuration introduced in §3.1, we instantiate per-model dimensions as listed in Table 2, where the hook block  $\ell$  is chosen from the middle-to-late transformer blocks of each model under zero-based indexing. Both training stages use AdamW [23] with a learning rate of  $5 \times 10^{-4}$ ,  $\beta = (0.9, 0.999)$ , a batch size of 16,384 tokens, and a warmup–stable–decay schedule (10%–80%–10%).

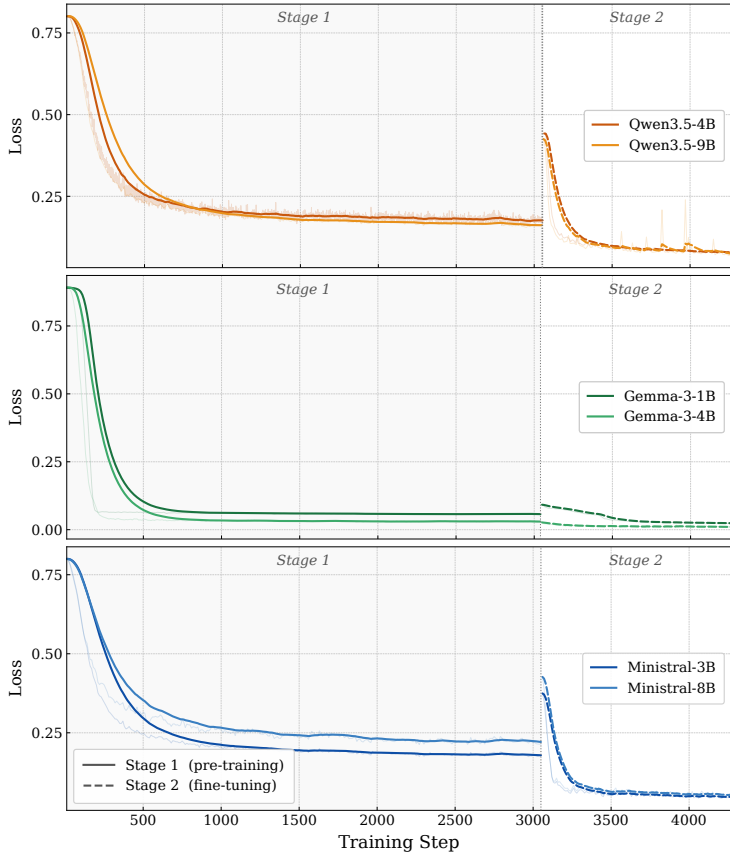


Figure 7: SAE reconstruction loss across the two-stage training curriculum, grouped by model family. Solid traces show Stage 1 (broad-corpus pre-training on OpenWebText2) and dashed traces show Stage 2 (When2Call adaptation), separated by the vertical divider. Light curves are raw per-step losses and bold curves are running averages. Within each panel, the two color shades distinguish the two model scales.

**Training diagnostics.** We monitor the SAE reconstruction loss throughout both training stages for each target model. Figure 7 groups the optimization traces by model family. Stage 1 losses drop

sharply within the first few hundred steps and then settle onto a stable plateau, indicating that the broad-corpus dictionary has converged on OpenWebText2. At the Stage 2 boundary the loss jumps because the residual-stream distribution shifts to When2Call, and then descends smoothly to a new plateau as the dictionary adapts to tool-use contexts. All six SAEs follow this pattern, confirming stable optimization across families and scales.

## B LLM as Judge Prompt

```

You are an expert at classifying responses from AI models.
Your task is to classify AI model's response into one of the following four
categories:

(1) direct_answer: The AI model responded to the User's questions based on its
existing knowledge, without requesting any additional information or using
external tools.

(2) tool_call: The AI model decided to use a tool from the provided ones to
help answer the question.

(3) request_for_info: The AI model requested additional information from the
User.

(4) cannot_answer: The AI model refused to answer the User's questions by
acknowledging the lack of required capabilities.

You should not judge whether the AI model's response is accurate or not. Only
provide the classification into one of these four categories.

<AVAILABLE_TOOLS> {tools} </AVAILABLE_TOOLS>
<USER_QUESTION> {question} </USER_QUESTION>
<AI_MODEL_RESPONSE> {response} </AI_MODEL_RESPONSE>

Please provide the classification in the following JSON format:
{"classification": "<direct_answer | tool_call | request_for_info |
cannot_answer>"}
Respond only in the prescribed JSON format.

```

## C Behavior-Labeled Discovery Set

We build the discovery set from the full When2Call evaluation split, running each target model on all contexts regardless of the original category. The LLM judge classifies each response into one of the four When2Call response types: `tool_call`, `request_for_info`, `direct_answer`, and `cannot_answer`. We then form  $\mathcal{D}^+$  from `tool_call` responses and  $\mathcal{D}^-$  from `request_for_info` responses. Responses in the other two categories describe plain answering and tool unavailability rather than the call/no-call gating decision and are excluded from the discovery set.

Table 3: Per-model response counts across the four When2Call categories assigned by the LLM judge. We form  $\mathcal{D}^+$  from `tool_call` responses and  $\mathcal{D}^-$  from `request_for_info` responses, and exclude the remaining two categories from the discovery set.

Model	tool_call	request_for_info	direct_answer	cannot_answer
Qwen3.5-4B	2163	751	272	466
Qwen3.5-9B	2151	758	257	486
Gemma-3-1b-it	3318	104	47	173
Gemma-3-4b-it	3037	223	207	185
Ministral-3-3B-Instruct	2408	603	363	278
Ministral-3-8B-Instruct	1993	731	382	546

Table 3 reports per-model counts of judged responses across the four categories. The first two columns correspond to  $|\mathcal{D}^+|$  and  $|\mathcal{D}^-|$ , whose cross-model variation reflects each model's response distribution.

## D Gating Feature Discovery Across Models

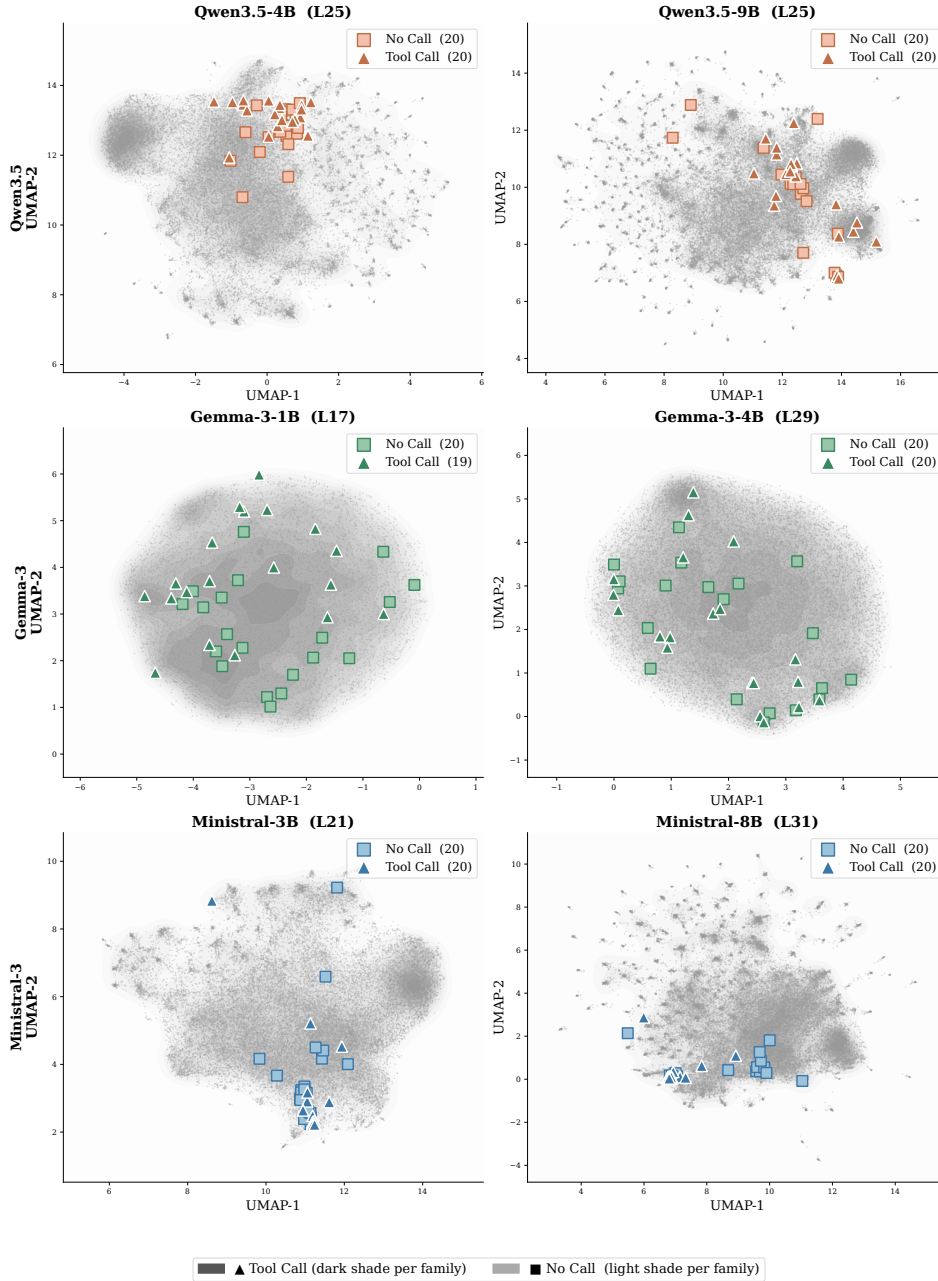


Figure 8: UMAP visualization of the SAE feature dictionary for each target model. Gray points are all SAE features projected to 2D, and the colored markers highlight the top-20 `TOOL_CALL` (triangles) and `NO_CALL` (squares) features returned by the discovery pipeline. Panel titles list the model name and the SAE hook layer.

Figure 8 situates the discovered gating features inside each SAE’s full feature dictionary. For the Qwen3.5 and Ministral-3 families, both `TOOL_CALL` and `NO_CALL` features collapse into a single tight cluster on the UMAP manifold, indicating that the call/no-call signal is concentrated in a coherent region of the SAE feature space. Gemma instead spreads its top features across most of the manifold, so gating information is carried by individually informative but geometrically dispersed directions. Despite this difference in feature geometry, the discovery pipeline returns a small, behavior-aligned feature set in all three families, consistent with the near-upper-bound probe AUROC reported in §3.3.

We further ask how the discovered features behave on failure cases. Figures 9, 10, and 11 contrast per-feature mean activations between Tool-Call-failure contexts (where the model wrongly issues a tool call) and No-Call-success contexts (where the model correctly withholds the tool call). Across all six target models, the top-ranked TOOL\_CALL features are systematically overactivated under failure and the top-ranked NO\_CALL features are systematically underactivated. This bidirectional shift is consistent with IBH: failures arise from a coordinated imbalance between the two feature groups rather than from a single group acting in isolation, and the pattern holds even where the UMAP geometry differs across families.

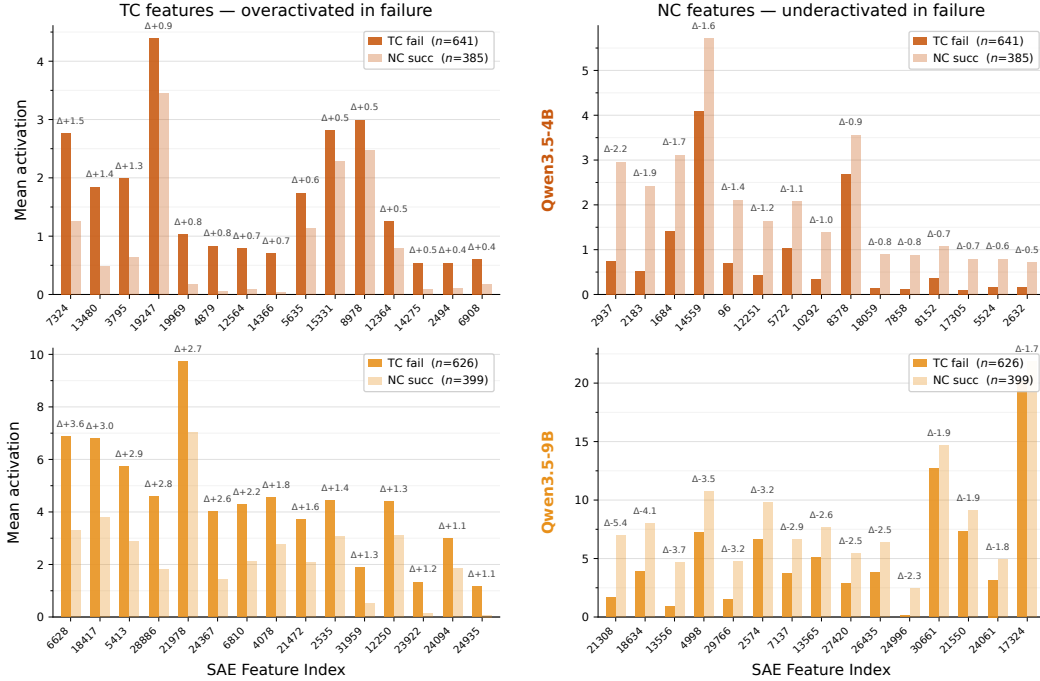


Figure 9: Per-feature mean SAE activation on Tool-Call-failure (over-calling) vs. No-Call-success contexts for Qwen3.5-4B (top) and Qwen3.5-9B (bottom), with top-ranked TOOL\_CALL features (left) overactivated and NO\_CALL features (right) underactivated under failure.

## E Adaptive Margin-Calibrated Steering Details

This section records the calibration and inference steps needed to reproduce the steering vectors, complementing the derivation in §5.1.

**Offline calibration.** For each target model, we cache residual-stream states at the selected SAE hook layer and the corresponding judged model decisions on the calibration set, encode each state with the model-specific SAE, and restrict to examples whose decision  $\hat{d}_x \in \{\text{CALL}, \text{NO\_CALL}\}$ . On this set, we compute the signed margin  $m_r(x)$  over the restricted basis  $\mathcal{C}_r \cup \mathcal{N}_r$  following the definition in §4.1, fit Eq. (9), and keep the candidate only when  $\beta_r > 0$  so that the margin orders CALL decisions in the expected direction. We then obtain  $\delta_r$  via Eq. (10), normalize feature weights as in Eq. (11), and form  $\mathbf{v}_r$  from Eq. (12). Each candidate budget  $r$  induces a distinct feature basis and bias estimate, so calibration is repeated independently for each value of  $r$ .

**Margin-shift approximation.** Decomposing the contribution of  $\mathbf{v}_r$  to the two sides of  $m_r$  under a local linear SAE approximation gives  $\Delta m_r \approx \alpha \delta_r + (1 - \alpha) \delta_r = \delta_r$ . Because decoder directions need not form an orthogonal basis, we treat this as a calibrated target and verify the realized margin shift when reporting steering results.

**Algorithm.** Algorithm 1 summarizes the full offline calibration and online inference procedure.

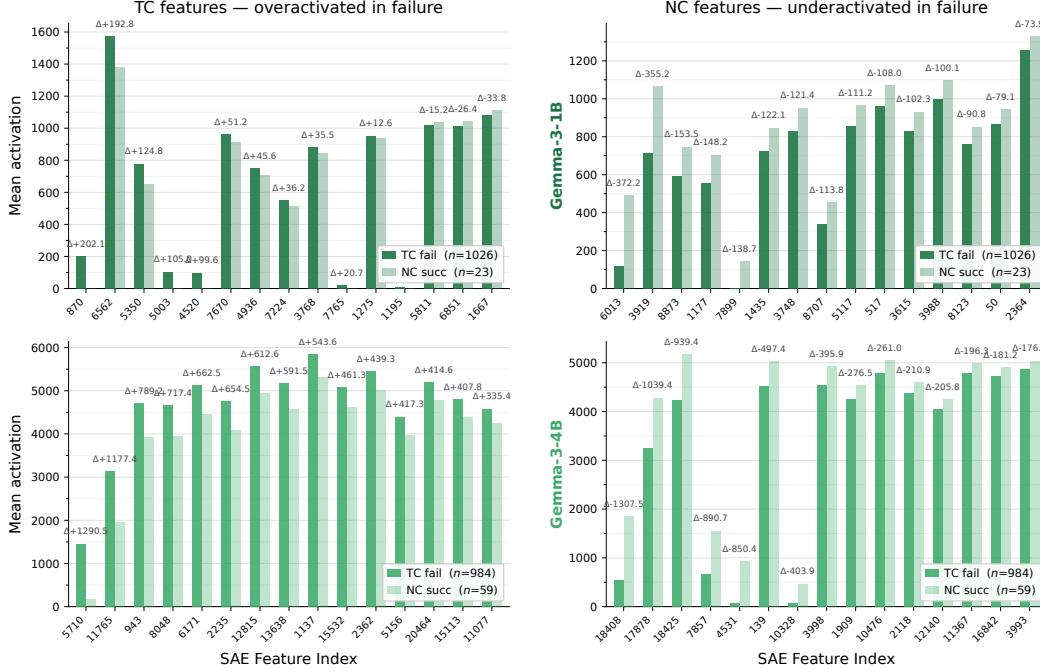


Figure 10: Per-feature mean SAE activation on Tool-Call-failure (over-calling) vs. No-Call-success contexts for Gemma-3-1B (top) and Gemma-3-4B (bottom), with top-ranked TOOL\_CALL features (left) overactivated and NO\_CALL features (right) underactivated under failure.

---

**Algorithm 1** Adaptive Margin-Calibrated Steering (AMCS)

---

**Require:** Cached hidden states  $\{\mathbf{h}_x\}_{x \in \mathcal{D}_{\text{cal}}}$ , cached model decisions  $\{\hat{d}_x\}$ , SAE encoder and decoder, hook layer  $\ell$ , feature rankings  $\mathcal{C}$  and  $\mathcal{N}$ , attribution gaps  $\{\Delta_j^{\mathcal{C}}\}$  and  $\{\Delta_j^{\mathcal{N}}\}$ , feature budget  $r$  and allocation coefficient  $\alpha$

**Ensure:** Steering vector  $\mathbf{v}_r$  and steered response  $\tilde{y}$

- 1: **Offline calibration**
  - 2: Select  $\mathcal{C}_r \leftarrow \text{Top}_r(\mathcal{C})$  and  $\mathcal{N}_r \leftarrow \text{Top}_r(\mathcal{N})$
  - 3: **for all**  $x \in \mathcal{D}_{\text{cal}}$  **do**
  - 4:    $\mathbf{z}_x \leftarrow \text{SAEEnc}(\mathbf{h}_x)$
  - 5:    $m_r(x) \leftarrow \frac{1}{r} \sum_{j \in \mathcal{C}_r} \|\mathbf{d}_j\|_2 z_{x,j} - \frac{1}{r} \sum_{j \in \mathcal{N}_r} \|\mathbf{d}_j\|_2 z_{x,j}$
  - 6: **end for**
  - 7:  $\mathcal{D}_{\text{bin}} \leftarrow \{x \in \mathcal{D}_{\text{cal}} : \hat{d}_x \in \{\text{CALL}, \text{NO\_CALL}\}\}$
  - 8: Fit  $\Pr(\hat{d} = 1 | m_r) = \sigma(\beta_r m_r + \beta_{0,r})$  on  $\mathcal{D}_{\text{bin}}$
  - 9: **if**  $\beta_r \leq 0$  **then return** SKIP
  - 10: **end if**
  - 11:  $\delta_r \leftarrow -\beta_{0,r}/\beta_r$  ▷ Eq. (10)
  - 12:  $\omega_j^{\mathcal{C}} \leftarrow |\Delta_j^{\mathcal{C}}| / \sum_{k \in \mathcal{C}_r} |\Delta_k^{\mathcal{C}}|$  for  $j \in \mathcal{C}_r$
  - 13:  $\omega_j^{\mathcal{N}} \leftarrow |\Delta_j^{\mathcal{N}}| / \sum_{k \in \mathcal{N}_r} |\Delta_k^{\mathcal{N}}|$  for  $j \in \mathcal{N}_r$
  - 14:  $\mathbf{v}_r \leftarrow \alpha r \delta_r \sum_{j \in \mathcal{C}_r} \omega_j^{\mathcal{C}} \mathbf{d}_j + (1 - \alpha) r (-\delta_r) \sum_{j \in \mathcal{N}_r} \omega_j^{\mathcal{N}} \mathbf{d}_j$
  - 15: **Online inference**
  - 16: Register a forward hook at layer  $\ell$  that applies  $\mathbf{H}_\ell \leftarrow \mathbf{H}_\ell + \mathbf{v}_r$
  - 17: Generate  $\tilde{y}$  with the hook active
  - 18: Remove the hook
  - 19: **return**  $\mathbf{v}_r, \tilde{y}$
- 

**Complexity.** For a fixed feature budget  $r$ , constructing  $\mathbf{v}_r$  requires a weighted sum of  $2r$  decoder columns and costs  $O(rd)$ . At inference time, AMCS adds one vector of dimension  $d$  to the hooked residual stream. It introduces no extra model calls, no iterative search over steering coefficients, and no additional learned parameters.

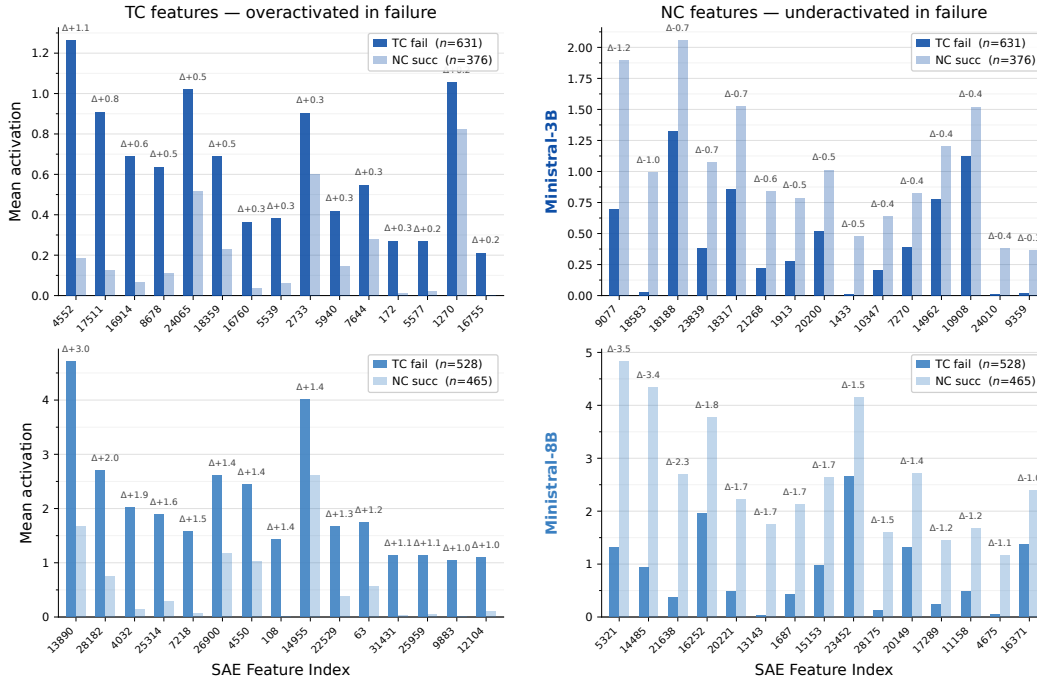


Figure 11: Per-feature mean SAE activation on Tool-Call-failure (over-calling) vs. No-Call-success contexts for Ministral-3-3B (top) and Ministral-8B (bottom), with top-ranked TOOL\_CALL features (left) overactivated and NO\_CALL features (right) underactivated under failure.

## F Perplexity of Steered Outputs

Table 4: Next-token perplexity of steered outputs on the When2Call test split. Baseline is the unmodified model. Suppress and Promote are one-sided ablations using only the call-suppression or no-call-promotion component of the AMCS vector, respectively. AMCS is the full two-sided intervention. The parameter  $\alpha \in \{0.2, 0.6, 1.0\}$  controls the allocation between the two sides. Extreme values for Gemma3 reflect the weak CALL/NO\_CALL feature separation noted in §5.2.

Method	$\alpha$	Qwen3.5-4B	Qwen3.5-9B	Gemma3-1B	Gemma3-4B	Ministral3-3B	Ministral3-8B
Baseline	–	1.32	1.37	1.04	1.02	3.17	2.93
Suppress	0.2	1.33	1.37	1.25	1.06	3.12	2.85
	0.6	1.36	1.39	$3.19 \times 10^7$	1.33	2.93	2.58
	1.0	1.45	1.42	225.02	57317.43	2.12	1.63
Promote	0.2	1.34	1.36	1.13	1.03	3.14	2.90
	0.6	1.37	1.35	2.38	1.20	3.09	2.84
	1.0	1.43	1.37	7.44	1.54	3.02	2.80
AMCS	0.2	1.36	1.38	2.29	1.02	3.08	2.90
	0.6	1.36	1.42	1.53	1.02	3.05	2.84
	1.0	1.38	1.46	392.70	1.02	3.01	2.80

Note that models use different prompt templates and produce responses of different types (TOOL\_CALL vs. NO\_CALL), so perplexity values are only meaningful within a single model compared against its own baseline, not across models or response types. For Qwen3.5 and Ministral3, all three methods maintain perplexity within a small margin of the unsteered baseline across all tested  $\alpha$  values, confirming that residual-stream additions do not destabilize generation. Gemma3 is the exception: Suppress at higher  $\alpha$  produces extreme values ( $3.19 \times 10^7$  for Gemma3-1B at  $\alpha = 0.6$ , 57317.43 for Gemma3-4B at  $\alpha = 1.0$ ), and AMCS at  $\alpha = 1.0$  also degrades for the 1B model (392.70). This instability mirrors the weak CALL/NO\_CALL feature separation already noted for Gemma3 in §5.2 and reinforces treating those models as reference cases.

## G LLM Usage

This work studies LLMs as target models for tool-use decisions. We also use an independent LLM judge to classify generated responses into `CALL` and `NO_CALL` behavior labels for feature discovery, calibration, and evaluation. The judge prompt is reported in Appendix B. The same judging procedure is used for baseline and steered conditions. AMCS itself is defined by SAE activations, a fitted margin model, and a fixed hook, rather than by an LLM component.

## H Broader Impacts

This work can improve the reliability and efficiency of tool-using agents by reducing unnecessary tool calls, especially in cases where the model should ask for missing information instead of calling a tool. Such behavior can lower API cost, reduce avoidable external actions, and make agent decisions easier to audit through feature-level diagnostics.

At the same time, steering a model’s tool-use propensity can introduce deployment risks if applied without task-specific validation. Overly conservative steering may suppress necessary tool calls, while overly aggressive steering may amplify automation errors. We therefore view AMCS as a diagnostic and mitigation tool that should be evaluated with call accuracy, no-call accuracy, and downstream task checks before deployment.

## I Experiments Compute Resources

All experiments were conducted on NVIDIA A800 (80GB) GPUs. For individual experiments, SAE training on a single model requires approximately 4 GPU-hours, while `WHEN2CALL` evaluation on a single model takes approximately 3 GPU-hours; experiments involving activation steering require approximately 4 GPU-hours per model. The main results in Table 1 encompass 98 `WHEN2CALL` evaluation runs, amounting to roughly  $4 \times 98 = 392$  GPU-hours in total, which were completed in approximately 2 days using 8 GPUs in parallel. In aggregate, all experiments reported in this paper were conducted over a period of two months with dedicated access to 8 GPUs.

```

SYSTEM
<|im_start|>system:# Tools. You have access to the following functions:
<tools>{"type": "function", "function": {"name": "get_current_time", "description": "Get the current time", "parameters": {"type": "object", "properties": {"timezone": {"type": "string", "description": "The timezone, e.g. America/New_York"}}, "required": ["timezone"]}}, {"type": "function", "function": {"name": "search_books", "description": "Search for books by title or author", "parameters": {"type": "object", "properties": {"keyword": {"type": "string", "description": "The keyword to search for in book titles or authors"}}, "required": ["keyword"]}}
</tools>
If you choose to call a function ONLY reply in the following format with NO suffix:
<tool_call>function=example_function_name<parameter=example_parameter_1>value_1</parameter><parameter=example_parameter_2>
This is the value for the second parameter that can span multiple lines
</parameter></function></tool_call>
<IMPORTANT>Reminder: Function calls MUST follow the specified format: an inner <function=...></function>
block must be nested within <tool_call></tool_call> XML tags. Required parameters MUST be specified. You
may provide optional reasoning for your function call in natural language BEFORE the function call, but NOT
after. If there is no function call available, answer the question like normal with your current knowledge
and do not tell the user about function calls.
</IMPORTANT><|im_end|>

USER
<|im_start|>user:What's the current time in New York?<|im_end|>

ASSISTANT
<|im_start|>assistant:<tool_call><function=get_current_time><parameter=timezone>America/New_York</
parameter></function></tool_call><|im_end|>

USER
<|im_start|>user:<tool_response>{"time": "10:00 AM"}</tool_response><|im_end|>

ASSISTANT
<|im_start|>assistant:The current time in New York is 10:00 AM.<|im_end|>

USER
<|im_start|>user:And what about in London?<|im_end|>

ASSISTANT
<|im_start|>assistant:<think>Okay, the user first asked for the current time in New York, and I used the
get_current_time tool with America/New_York. Now they're asking "And what about in London?" so they want the time
in London. I need to check the available tools. The get_current_time function requires a timezone. London's
timezone is Europe/London. I should call the same function but with the Europe/London timezone parameter.
Make sure to structure the tool call correctly. The parameters need to be a JSON object with the timezone. So
the arguments should be {"timezone": "Europe/London"}. Double-check the timezone name. Yes, it's Europe/L
ondon for London, UK. No daylight saving adjustments needed here since the tool probably handles that
automatically based on the timezone string. So the correct tool call is get_current_time with Europe/London.
</think><tool_call><function=get_current_time><parameter=timezone>Europe/London</parameter></function>
</tool_call><|im_end|>

```

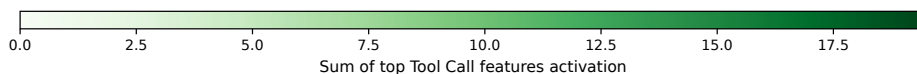


Figure 12: Token-level attribution of the top-10 TOOL\_CALL features on a representative context where the model correctly issues a tool call. Green intensity is proportional to each token's contribution to the summed feature activation (x-axis). The strongest signal concentrates in the tool schema definitions and the user query, consistent with these features encoding tool-invocation intent.



Figure 13: Token-level attribution of the top-10 NO\_CALL features on a representative context where the model correctly withholds a tool call and requests missing information instead. Red intensity is proportional to each token’s contribution to the summed feature activation (x-axis). The signal concentrates in the underspecified user query and tool schema, consistent with these features encoding information-insufficiency.